Natural Hazards (2023) 116:637–662
https://doi.org/10.1007/s11069-022-05692-2

ORIGINAL PAPER

Extratropical cyclone damage to the seawall in Dawlish, UK: eyewitness accounts, sea level analysis and numerical modelling

Keith Adams[1] · **Mohammad Heidarzadeh**[2]

Received: 17 May 2022 / Accepted: 17 October 2022 / Published online: 14 November 2022

Abstract
The February 2014 extratropical cyclonic storm chain, which impacted the English Channel (UK) and Dawlish in particular, caused significant damage to the main railway connecting the south-west region to the rest of the UK. The incident caused the line to be closed for two months, £50 million of damage and an estimated £1.2bn of economic loss. In this study, we collate eyewitness accounts, analyse sea level data and conduct numerical modelling in order to decipher the destructive forces of the storm. Our analysis reveals that the disaster management of the event was successful and efficient with immediate actions taken to save lives and property before and during the storm. Wave buoy analysis showed that a complex triple peak sea state with periods at 4–8, 8–12 and 20–25 s was present, while tide gauge records indicated that significant surge of up to 0.8 m and wave components of up to 1.5 m amplitude combined as likely contributing factors in the event. Significant impulsive wave force of up to 286 KN was the most likely initiating cause of the damage. Reflections off the vertical wall caused constructive interference of the wave amplitudes that led to increased wave height and significant overtopping of up to 16.1 $m^3/s/m$ (per metre width of wall). With this information and our engineering judgement, we conclude that the most probable sequence of multi-hazard cascading failure during this incident was: wave impact force leading to masonry failure, loss of infill and failure of the structure following successive tides.

Keywords Storm surge · Cyclone · Railway · Climate change · Infrastructure · Resilience

✉ Keith Adams
keith.adams2@brunel.ac.uk
https://www.brunel.ac.uk/people/keith-adams1

[1] Department of Civil and Environmental Engineering, Brunel University London, Uxbridge UB8 3PH, UK

[2] Department of Architecture and Civil Engineering, University of Bath, Bath BA2 7AY, UK

1 Introduction

The progress of climate change and increasing sea levels has started to have wide ranging effects on critical engineering infrastructure (Shakou et al. 2019). The meteorological effects of increased atmospheric instability linked to warming seas mean we may be experiencing more frequent extreme storm events and more frequent series or chains of events, as well as an increase in the force of these events, a phenomenon called storminess (Mölter et al. 2016; Feser et al. 2014). Features of more extreme weather events in extratropical latitudes (30°–60°, north and south of the equator) include increased gusting winds, more frequent storm squalls, increased prolonged precipitation and rapid changes in atmospheric pressure and more frequent and significant storm surges (Dacre and Pinto 2020). A recent example of these events impacting the UK with simultaneous significant damage to coastal infrastructure was the extratropical cyclonic storm chain of winter 2013/2014 (Masselink et al. 2016; Adams and Heidarzadeh 2021). The cluster of storms had a profound effect on both coastal and inland infrastructure, bringing widespread flooding events and large insurance claims (RMS 2014).

The extreme storms of February 2014, which had a catastrophic effect on the seawall of the south Devon stretch of the UK's south-west mainline, caused a two-month closure of the line and significant disruption to the local and regional economy (Fig. 1b) (Network Rail 2014; Dawson et al. 2016; Adams and Heidarzadeh 2021). Restoration costs were £35 m, and economic effects to the south-west region of England were estimated up to £1.2bn (Peninsula Rail Taskforce 2016). Adams and Heidarzadeh (2021) investigated the disparate cascading failure mechanisms which played a part in the failure of the railway through Dawlish and attempted to put these in the context of the historical records of infrastructure damage on the line. Subsequent severe storms in 2016 in the region have continued to cause damage and disruption to the line in the years since 2014 (Met Office 2016). Following the events of 2014, Network Rail[1] who owns the network has undertaken a resilience study. As a result, it has proposed a £400 m refurbishment of the civil engineering assets that support the railway (Fig. 1) (Network Rail 2014). The new seawall structure (Fig. 1a,c), which is constructed of pre-cast concrete sections, encases the existing Brunel seawall (named after the project lead engineer, Isambard Kingdom Brunel) and has been improved with piled reinforced concrete foundations. It is now over 2 m taller to increase the available crest freeboard and incorporates wave return features to minimise wave overtopping. The project aims to increase both the resilience of the assets to extreme weather events as well as maintain or improve amenity value of the coastline for residents and visitors.

In this work, we return to the Brunel seawall and the damage it sustained during the 2014 storms which affected the assets on the evening of the 4th and daytime of the 5th of February and eventually resulted in a prolonged closure of the line. The motivation for this research is to analyse and model the damage made to the seawall and explain the damage mechanisms in order to improve the resilience of many similar coastal structures in the UK and worldwide. The innovation of this work is the multidisciplinary approach that we take comprising a combination of analysis of eyewitness accounts (social science), sea level and wave data analysis (physical science) as well as numerical modelling and engineering judgement (engineering sciences). We investigate the contemporary wave climate

[1] https://www.networkrail.co.uk/..

Fig. 1 Location of Dawlish railway station. **a** The completed section of the new seawall looking towards the train station along King Harry's Walk (Completed first section of Dawlish seawall at dusk (networkrailmediacentre.co.uk)). **b** An aerial view of the seawall damage sustained at Riviera Terrace in February 2014 (Dawlish aerial view of 2014 damage (networkrailmediacentre.co.uk)). **c** Waves impacting the newly constructed seawall south of the station, now 2.5 m taller with an integrated wave return (The completed first section of new seawall effectively deflecting waves back out to sea (networkrailmediacentre.co.uk))

and sea levels by interrogating the real-time tide gauge and wave buoys installed along the south-west coast of the English Channel. We then model a typical masonry seawall (Fig. 2), applying the computational fluid dynamics package FLOW3D-Hydro,[2] to quantify the magnitude of impact forces that the seawall would have experienced leading to its failure. We triangulate this information to determine the probable sequence of failures that led to the disaster in 2014.

2 Data and methods

Our data comprise eyewitness accounts, sea level records from coastal tide gauges and offshore wave buoys as well as structural details of the seawall. As for methodology, we analyse eyewitness data, process and investigate sea level records through Fourier transform

[2] https://www.flow3d.com/products/flow-3d-hydro/.

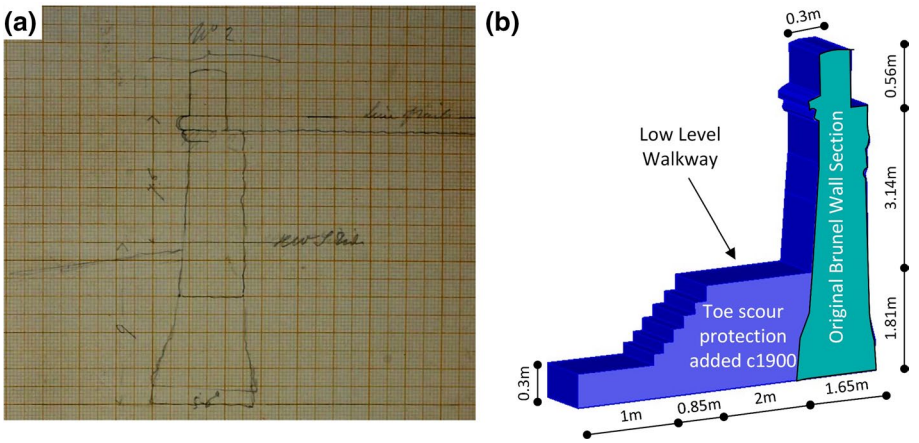

Fig. 2 **a** An original sketch of the Dawlish seawall made by the lead Engineer Mr Brunel around 1844–46 (Brunel Institute, 2022). **b** The 3D wall model created for our numerical simulations based on Brunel's sketch and subsequent additions of toe reinforcement for scour protection and low-level walkway

and conduct numerical simulations using the Flow3D-Hydro package (Flow Science 2022). Details of the data and methodology are provided in the following.

2.1 Eyewitness data

The scale of damage to the seawall and its effects led the local community to document the first-hand accounts of those most closely affected by the storms including residents, local businesses, emergency responders, politicians and engineering contractors involved in the post-storm restoration work. These records now form a permanent exhibition in the local museum in Dawlish[3], and some of these accounts have been transcribed into a DVD account of the disaster (Dawlish Museum 2015). We have gathered data from the Dawlish Museum, national and international news reports, social media tweets and videos. Table 1 provides a summary of the eyewitness accounts. Overall, 26 entries have been collected around the time of the incident. Our analysis of the eyewitness data is provided in the third column of Table 1 and is expanded in Sect. 3.

2.2 Sea level data and wave environment

Our sea level data are a collection of three tide gauge stations (Newlyn, Devonport and Swanage Pier—Fig. 5a) owned and operated by the UK National Tide and Sea Level Facility[4] for the Environment Agency and four offshore wave buoys (Dawlish, West Bay, Torbay and Chesil Beach—Fig. 6a). The tide gauge sites are all fitted with POL-EKO (www.pol-eko.com.pl) data loggers. Newlyn has a Munro float gauge with one full tide and one mid-tide pneumatic bubbler system. Devonport has a three-channel data pneumatic bubbler

[3] https://www.devonmuseums.net/Dawlish-Museum/Devon-Museums/.
[4] https://ntslf.org/.

Table 1 Eyewitness accounts of damage to the Dawlish railway due to the February 2014 storm and our interpretations

Date (dd/mm/yy)	Eyewitness accounts	Analysis and observations	References
04/02/2014	Flooding of town centre, river overflowing, wind and waves inundating at various points along the seawall especially near centre of town. (1400 h)	Surge and waves were intensive causing overtopping of the wall	Dawlish Museum (2015)
	Network Rail shuts the mainline down. First Great Western (the railway company) cancel all trains after some engines get stranded and battered on the down line by large storm waves. (1515 h)	Severe overtopping of the seawall and inundation	Dawlish Museum (2015)
	Town centre damage reported	Strong wave actions and inundations	BBC (2014a)
	The road "Sea Lawn terrace"– report of house flooding by resident to fire service due to high wind and waves. A car is stranded and has water inundation along Marine Parade (the coastal road)	Severe coastal flooding along Marine Parade	Dawlish Museum (2015)
	"Roof rattling, roof tiles, doors and windows leaking water". (Sea Lawn Terrace, 1800 h)	Winds and wave overtopping cause structural damage to houses fronting the sea at Sea Lawn Terrace	Chris Saich, local resident (BBC, 2014b)
	Fire station manager reports the cliffs being threatened at various points east of Dawlish towards the Warren due to large waves	The storm cascades to other hazards such as coastal landslides	Robert Porch, Dawlish Fire Station Manager (Dawlish Museum 2015)
	Road already collapsed, gas mains have been broken, smell of leaking gas by fire service along Sea Lawn Terrace	Cascading hazards of energy line failures and damage to energy infrastructure along Sea Lawn Terrace	Robert Porch (Dawlish Museum 2015)
	Sea Lawn Lodge guest house, signs blown down. (2100 h)	Strong gusting wind, as a result of the storm, causing damage	Gerard Belcher, Owner of Sea Lawn Lodge (Dawlish Museum 2015)
	Rivera terrace is evacuated, concern over houses being vulnerable. (2115 h)	Local police declare major incident and arrange evacuation of local residents	Dawlish Museum (2015)
	Reports of ballast having been washed away, rail line hanging in mid-air along Sea Lawn Terrace	Severe damage to railway infrastructure along Sea Lawn Terrace	Dawlish Museum (2015)
	Police ask Sea Lawn Lodge (a local hotel) to act as clearing house for evacuated residents, police in attendance to take registration of all residents and search for missing persons. (2300 h)	Temporary evacuation centre for local people	Gerard Belcher, (Dawlish Museum 2015)

Table 1 (continued)

Date (dd/mm/yy)	Eyewitness accounts	Analysis and observations	References
	"Water coming through windows, down the chimney into our lounge" along Sea Lawn Terrace. Evacuation by local police. (2300 h)	Wave overtopping and impact forces so severe, ballast is breaking windows and water ingress down chimney suggests water reaching in excess of 10 m above wall base level along Sea Lawn Terrace	Chris Saich, local resident (BBC 2014c)
	Police evacuation for River Terrace—"it was like an earthquake, the houses were jumping up and down on their footings … it wasn't a storm, it was a hurricane". (2345 h)	Local residents, used to coastal storms, identify this event as extreme and liken it to a hurricane	Robert Parker, local resident (BBC, 2014c)
05/02/2014	Local Leisure Centre re-purposed for resident evacuation. (0200 h)	Temporary evacuation centre for local people	Gerard Belcher, (Dawlish Museum 2015)
	80 mph winds. (0700 h)	Strong gusting wind	
	Riviera Terrace Seawall gone; 1st storm was abating. Took some pictures pre-dawn. (0744 h)	This is done by David Crome (First Great Western General Manager—West)	Steve Briers, BBC Cameraman and Resident (Dawlish Museum 2015)
	As morning went on, the hole in the wall got bigger and bigger as waves wash away more infill material and undermine road asphalt etc	As seen in Fig. 1b, the storm has caused major damage to the railway and line was washed away	Steve Briers (Dawlish Museum 2015)
	Station platform, structure being seriously damaged by wind and waves	Damage to the station	Dawlish Museum (2015)
	Coastal Road flooded due to storm surge	Continuing coastal flooding	Dawlish Museum (2015)
	Marine Parade (a coastal road), shifting ballast traps cars and knocks down railings on town side	The debris from railway damage impacted the nearby road and caused damage	Dawlish Museum (2015)
	Seawall along the frontage near the viaduct is breached in many sections	Direct wave damage to the seawall	Dawlish Museum (2015)
	Marine Parade (a coastal road) extensive damage to tracks and ballast	Wave overtopping damage	Dawlish Museum (2015)
	Boat cove—many beach huts destroyed, blocking the access to the cove	Coastal inundation	Dawlish Museum (2015)
	5000 t concrete poured, 150 t steel. Pumping through 100 mm pipes from town to site of damage	Initial temporary repair work	Gerard Belcher, (Dawlish Museum 2015)

Table 1 (continued)

Date (dd/mm/yy)	Eyewitness accounts	Analysis and observations	References
	Breaches of wall reported from Dawlish Warren to Coryton Cove. 300 engineers working costing a total of £15 m	Continuing damage due to gusting wind and wave overtopping	Dawlish Museum (2015)
	"Biggest structural engineering feat in the southwest in the last decade … worst damage ever seen to the seawall in the local engineers' careers"	Evaluation of the storm suggests this was an extreme event with multiple cascading hazards activated	Patrick Hallgate, Network Rail Engineer (BBC 2014a)

system, and Swanage Pier consists of a pneumatic gauge. Each has a sampling interval of 15 min, except for Swanage Pier which has a sampling interval of 10 min. The tide gauges are located within the port areas, whereas the offshore wave buoys are situated approximately 2—3.3 km from the coast at water depths of 10–15 m. The wave buoys are all Datawell Wavemaker Mk III units[5] and come with sampling interval of 0.78 s. The buoys have a maximum saturation amplitude of 20.5 m for recording the incident waves which implies that every wave larger than this threshold will be recorded at 20.5 m. The data are provided by the British Oceanographic Data Centre[6] for tide gauges and the Channel Coastal Observatory[7] for wave buoys.

2.3 Sea level analysis

The sea level data underwent quality control to remove outliers and spikes as well as gaps in data (e.g. Heidarzadeh et al. 2022; Heidarzadeh and Satake 2015). We processed the time series of the sea level data using the Matlab signal processing tool (MathWorks 2018). For calculations of the tidal signals, we applied the tidal package TIDALFIT (Grinsted 2008), which is based on fitting tidal harmonics to the observed sea level data. To calculate the surge signals, we applied a 30-min moving average filter to the de-tided data in order to remove all wind, swell and infra-gravity waves from the time series. Based on the surge analysis and the variations of the surge component before the time period of the incident, an error margin of approximately ± 10 cm is identified for our surge analysis. Spectral analysis of the wave buoy data is performed using the fast Fourier transform (FFT) of Matlab package (Mathworks 2018).

2.4 Numerical modelling

Numerical modelling of wave-structure interaction is conducted using the computational fluid dynamics package Flow3D-Hydro version 1.1 (Flow Science 2022). Flow3D-Hydro solves the transient Navier–Stokes equations of conservation of mass and momentum using a finite difference method and on Eulerian and Lagrangian frameworks (Flow Science 2022). The aforementioned governing equations are:

$$\nabla . u = 0 \tag{1}$$

$$\frac{\partial u}{\partial t} + u.\nabla u = \frac{-\nabla P}{\rho} + \upsilon \nabla^2 u + g \tag{2}$$

where u is the velocity vector, P is the pressure, ρ is the water density, υ is the kinematic viscosity and g is the gravitational acceleration. A Fractional Area/Volume Obstacle Representation (FAVOR) is adapted in Flow3D-Hydro, which applies solid boundaries within the Eulerian grid and calculates the fraction of areas and volume in partially blocked volume in order to compute flows on corresponding boundaries (Hirt and Nichols 1981). We validated the numerical modelling through comparing the results with Sainflou's analytical

[5] https://www.datawell.nl/Products/Buoys/DirectionalWaveriderMkIII.aspx.
[6] https://www.bodc.ac.uk/.
[7] https://coastalmonitoring.org/cco/.

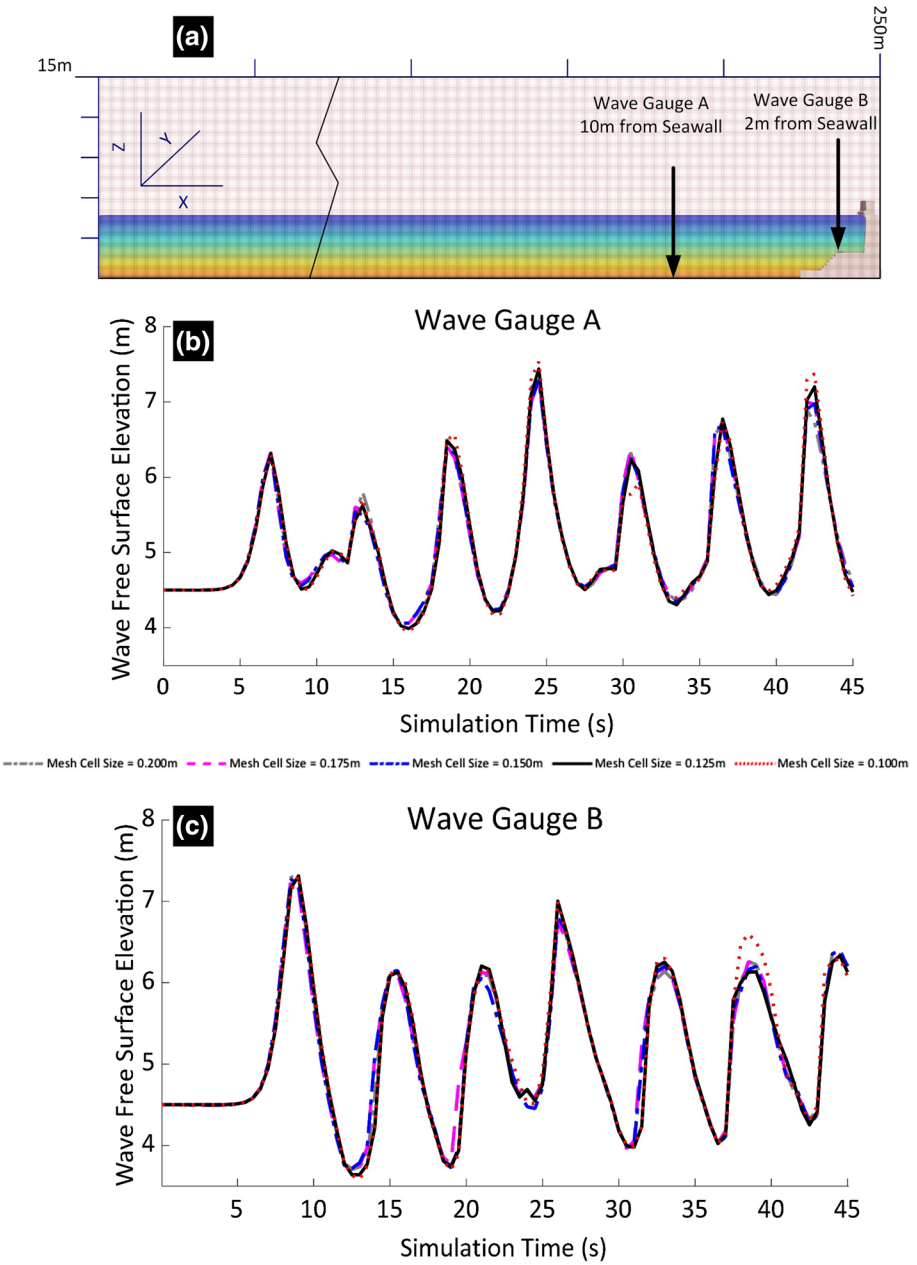

Fig. 3 **a** The model seawall computational domain showing the location of two gauges A and B, where wave time series are recorded (not to scale). **b** and **c** Time series of wave oscillations at the gauges A and B considering different mesh cell sizes

equation for the design of vertical seawalls (Sainflou 1928; Ackhurst 2020), which is as follows:

$$p_d = \frac{\rho g H \cosh k(d+z)}{\cosh kd} \cos \sigma t \tag{3}$$

where p_d is the hydrodynamic pressure, ρ is the water density, g is the gravitational acceleration, H is the wave height, d is the water depth, k is the wavenumber, z is the difference in still water level and mean water level, σ is the angular frequency and t is the time. The Sainflou's equation (Eq. 3) is used to calculate the dynamic pressure from wave action, which is combined with static pressure on the seawall.

Using Flow3D-Hydro, a model of the Dawlish seawall was made with a computational domain which is 250.0 m in length, 15.0 m in height and 0.375 m in width (Fig. 3a). The computational domain was discretised using a single uniform grid with a mesh size of 0.125 m. The model has a wave boundary at the left side of the domain (x-min), an outflow boundary on the right side (x-max), a symmetry boundary at the bottom (z-min) and a wall boundary at the top (z-max). A wall boundary implies that water or waves are unable to pass through the boundary, whereas a symmetry boundary means that the two edges of the boundary are identical and therefore there is no flow through it. The water is considered incompressible in our model. For volume of fluid advection for the wave boundary (i.e. the left-side boundary) in our simulations, we utilised the "Split Lagrangian Method", which guarantees the best accuracy (Flow Science, 2022).

The stability of the numerical scheme is controlled and maintained through checking the Courant number (C) as given in the following:

$$C = \frac{V \Delta t}{\Delta x} \tag{4}$$

where V is the velocity of the flow, Δt is the time step and Δx is the spatial step (i.e. grid size). For stability and convergence of the numerical simulations, the Courant number must be sufficiently below one (Courant et al. 1928). This is maintained by a careful adjustment of the Δx and Δt selections. Flow3D-Hydro applies a dynamic Courant number, meaning the program adjusts the value of time step (Δt) during the simulations to achieve a balance between accuracy of results and speed of simulation. In our simulation, the time step was in the range $\Delta t = 0.0051$—0.051 s.

In order to achieve the most efficient mesh resolution, we varied cell size for five values of $\Delta x = 0.1$ m, 0.125 m, 0.15 m, 0.175 m and 0.20 m. Simulations were performed for all mesh sizes, and the results were compared in terms of convergence, stability and speed of simulation (Fig. 3). A linear wave with an amplitude of 1.5 m and a period of 6 s was used for these optimisation simulations. We considered wave time histories at two gauges A and B and recorded the waves from simulations using different mesh sizes (Fig. 3). Although the results are close (Fig. 3), some limited deviations are observed for larger mesh sizes of 0.20 m and 0.175 m. We therefore selected mesh size of 0.125 m as the optimum, giving an extra safety margin as a conservative solution.

The pressure from the incident waves on the vertical wall is validated in our model by comparing them with the analytical equation of Sainflou (1928), Eq. (3), which is one of the most common set of equations for design of coastal structures (Fig. 4). The model was tested by running a linear wave of period 6 s and wave amplitude of 1.5 m against the wall, with a still water level of 4.5 m. It can be seen that the model results are very close to those from analytical equations of Sainflou (1928), indicating that our numerical model is accurately modelling the wave-structure interaction (Fig. 4).

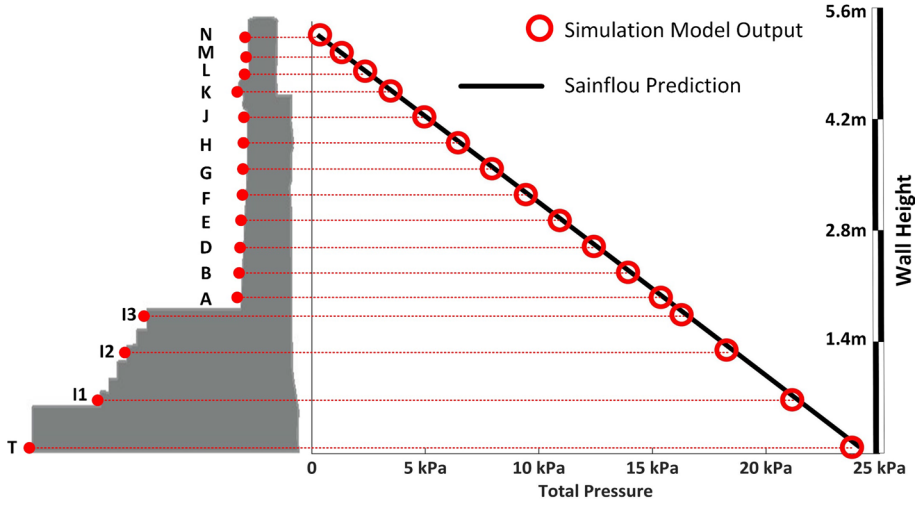

Fig. 4 Validation of the computer model seawall showing the probe locations (with identifiers) where pressures are recorded and comparison of the simulated pressures for a linear wave (red circles) with those calculated using the theoretical equations of Sainflou (1928) (black line)

3 Eyewitness account analysis

Contemporary reporting of the 4th and 5th February 2014 storms by the main national news outlets in the UK highlights the extreme nature of the events and the significant damage and disruption they were likely to have on the communities of the south-west of England. In interviews, this was reinforced by Network Rail engineers who, even at this early stage, were forecasting remedial engineering works to last for at least 6 weeks. One week later, following subsequent storms the cascading nature of the events was obvious. Multiple breaches of the seawall had taken place with up to 35 separate landslide events and significant damage to parapet walls along the coastal route also were reported. Residents of the area reported extreme effects of the storm, one likening it to an earthquake and reporting water ingress through doors windows and even through vertical chimneys (Table 1). This suggests extreme wave overtopping volumes and large wave impact forces. One resident described the structural effects as: "the house was jumping up and down on its footings".

Disaster management plans were quickly and effectively put into action by the local council, police service and National Rail. A major incident was declared, and decisions regarding evacuation of the residents under threat were taken around 2100 h on the night of 4th February when reports of initial damage to the seawall were received (Table 1). Local hotels were asked to provide short-term refuge to residents while local leisure facilities were prepared to accept residents later that evening. Initial repair work to the railway line was hampered by successive high spring tides and storms in the following days although significant progress was still made when weather conditions permitted (Table 1).

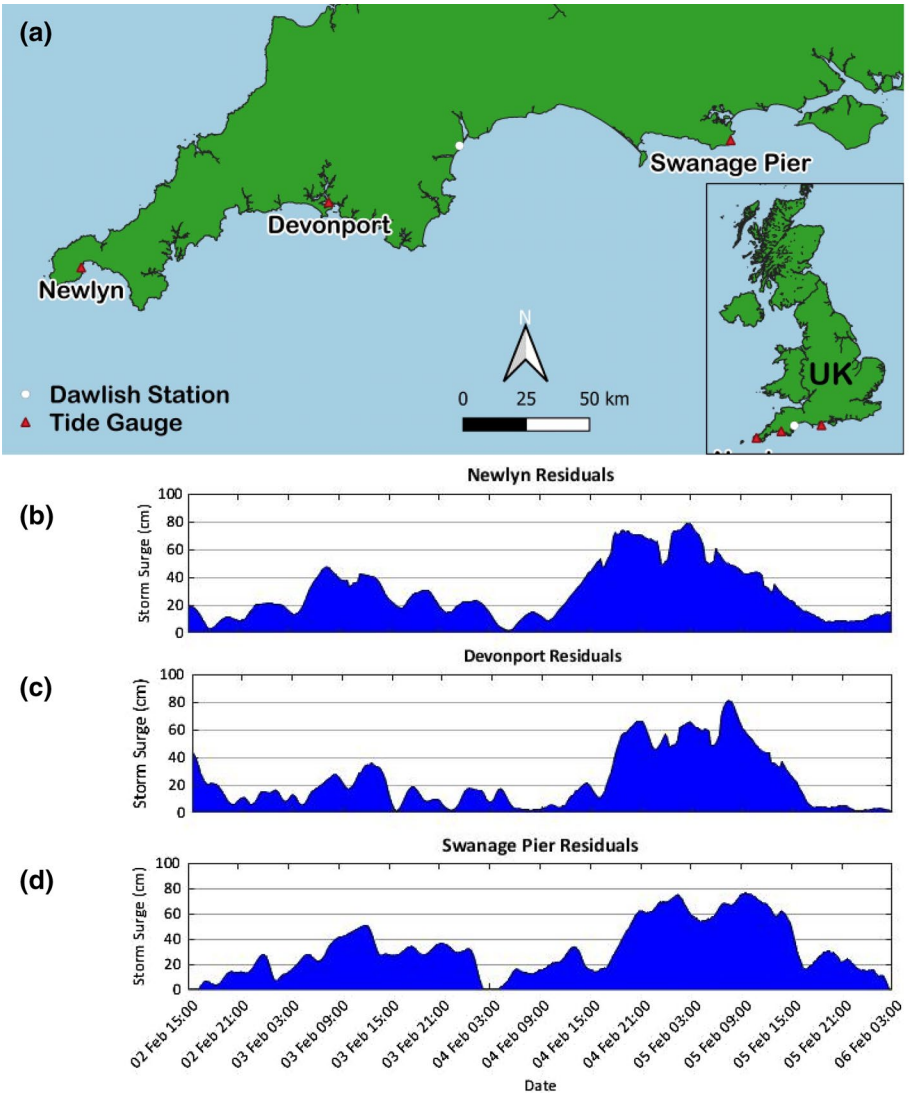

Fig. 5 **a** Area map showing the locations of tide gauges examined in this study. **b, c, d** The surge signals calculated at different tide gauge stations

4 Sea level observations and spectral analysis

The results of surge and wave analyses are presented in Figs. 5 and 6. A surge height of up to 0.8 m was recorded in the examined tide gauge stations (Fig. 5b-d). Two main episodes of high surge heights are identified: the first surge started on 3rd February 2014 at 03:00 (UTC) and lasted until 4th of February 2014 at 00:00; the second event occurred in the period 4th February 2014 15:00 to 5th February 2014 at 17:00 (Fig. 5b-d). These data imply surge durations of 21 h and 26 h for the first and the second events, respectively.

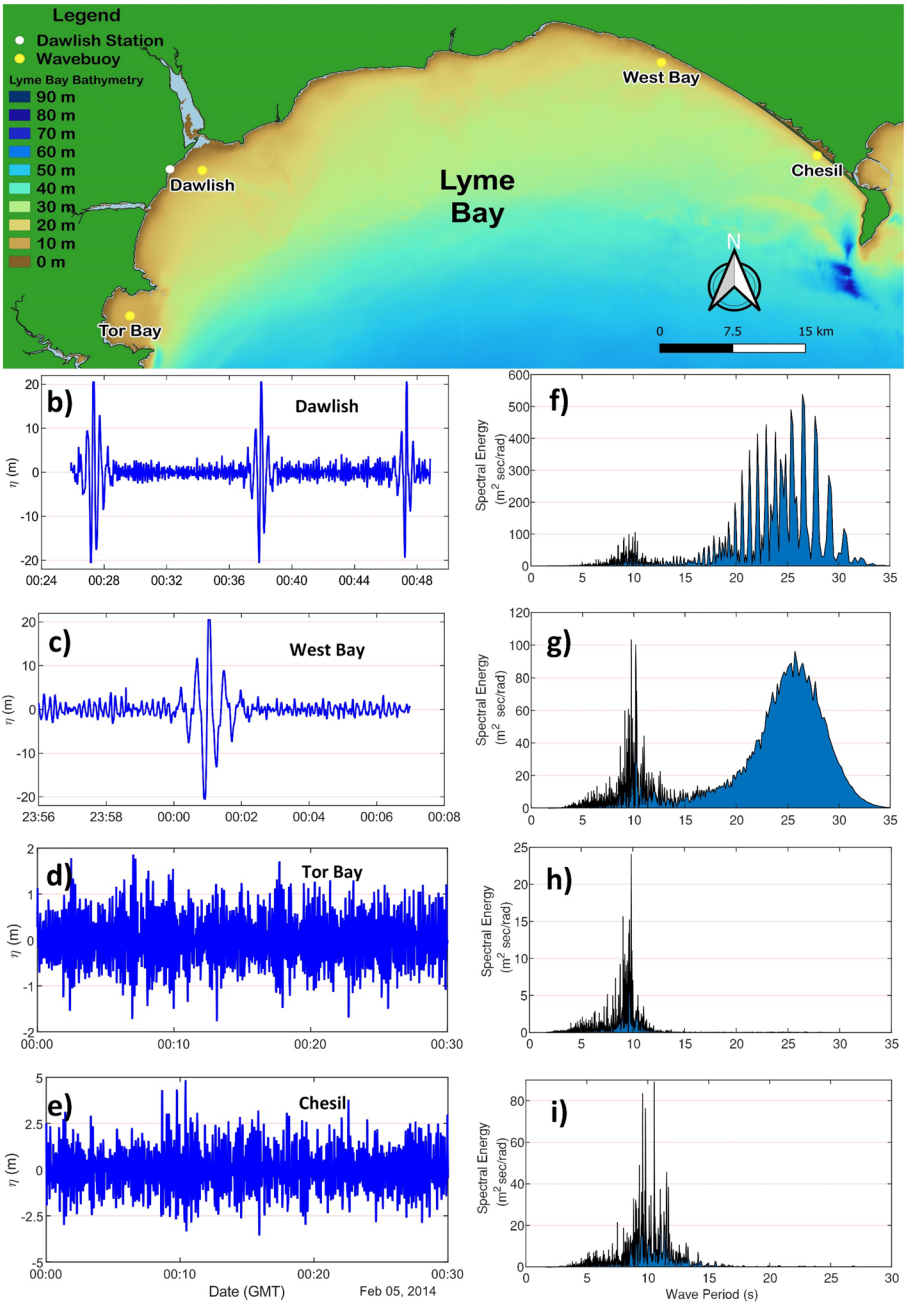

Fig. 6 **a** Area map showing the locations of wave buoys examined in this study. **b, c, d, e** Sea level oscillations recorded at wave buoys at different locations. **f, g, h, i** Corresponding spectra for each sea level record

Based on the surge data in Fig. 5, we note that the storm event of early February 2014 and the associated surges was a relatively powerful one, which impacted at least 230 km of the south coast of England, from Land's End to Weymouth, with large surge heights.

Based on wave buoy records, the maximum recorded amplitudes are at least 20.5 m in Dawlish and West Bay, 1.9 m in Tor Bay and 4.9 m in Chesil (Fig. 6a-b). The buoys at Tor Bay and Chesil recorded dual peak period bands of 4–8 and 8–12 s, whereas at Dawlish and West Bay registered triple peak period bands at 4–8, 8–12 and 20–25 s (Fig. 6c, d). It is important to note that the long-period waves at 20–25 s occur with short durations (approximately 2 min) while the waves at the other two bands of 4–8 and 8–12 s appear to be present at all times during the storm event.

The wave component at the period band of 4–8 s can be most likely attributed to normal coastal waves while the one at 8–12 s, which is longer, is most likely the swell component of the storm. Regarding the third component of the waves with long period of 20 -25 s, which occurs with short durations of 2 min, there are two hypotheses; it is either the result of a local (port and harbour) and regional (the Lyme Bay) oscillations (eg. Rabinovich 1997; Heidarzadeh and Satake 2014; Wang et al. 1992), or due to an abnormally long swell. To test the first hypothesis, we consider various water bodies such as Lyme Bay (approximate dimensions of 70 km × 20 km with an average water depth of 30 m; Fig. 6), several local bays (approximate dimensions of 3.6 km × 0.6 km with an average water depth of 6 m) and harbours (approximate dimensions of 0.5 km × 0.5 km with an average water depth of 4 m). Their water depths are based on the online Marine navigation website.[8] According to Rabinovich (2010), the oscillation modes of a semi-enclosed rectangle basin are given by the following equation:

$$T_{mn} = \frac{2}{\sqrt{gd}}\left[\left(\frac{m}{2L}\right)^2 + \left(\frac{n}{W}\right)^2\right]^{-1/2} \tag{5}$$

where T_{mn} is the oscillation period, g is the gravitational acceleration, d is the water depth, L is the length of the basin, W is the width of the basin, $m = 1, 2, 3, \ldots$ and $n = 0, 1, 2, 3, \ldots$; m and n are the counters of the different modes. Applying Eq. (5) to the aforementioned water bodies results in oscillation modes of at least 5 min, which is far longer than the observed period of 20–25 s. Therefore, we rule out the first hypothesis and infer that the long period of 20–25 s is most likely a long swell wave coming from distant sources. As discussed by Rabinovich (1997) and Wang et al. (2022), comparison between sea level spectra before and after the incident is a useful method to distinguish the spectrum of the weather event. A visual inspection of Fig. 6 reveals that the forcing at the period band of 20–25 s is non-existent before the incident.

5 Numerical simulations of wave loading and overtopping

Based on the results of sea level data analyses in the previous section (Fig. 6), we use a dual peak wave spectrum with peak periods of 10.0 s and 25.0 s for numerical simulations because such a wave would be comprised of the most energetic signals of the storm. For variations of water depth (2.0–4.0 m), coastal wave amplitude (0.5–1.5 m) (Fig. 7) and

[8] https://webapp.navionics.com/#boating@8&key=iactHlwfP.

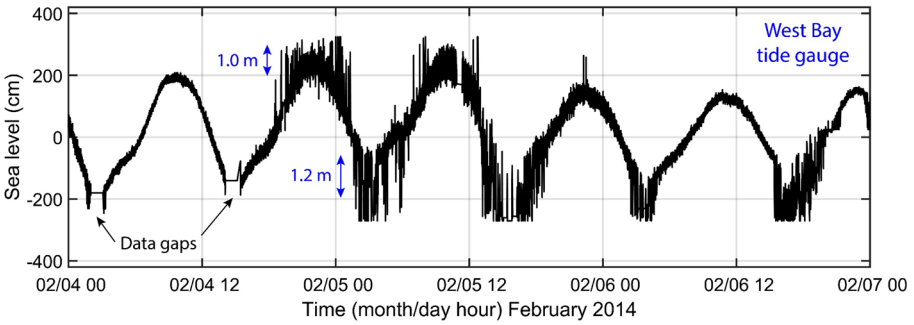

Fig. 7 Oscillations of wave (high-frequency oscillations) and tide (low-frequency oscillations with 12-h recurrence) at the West Bay tide gauge station

Table 2 The 20 scenarios considered for numerical simulations in this study

Scenario	Water depth (m)	Storm surge (m)	Effective water depth—d_{eff} (m)	Wave amplitude (m)	Maximum overtopping flowrate Q_{ov} (m^3/s/m)	Maximum force (KN)
1	4.0	0.5	4.5	0.5	4.5	171
2	3.0	0.5	3.5	0.5	3.8	138
3	2.0	0.5	2.5	0.5	n/a	92
4	2.5	0.5	3.0	0.5	n/a	108
5	3.5	0.5	4.0	0.5	1.2	151
6	2.0	0.8	2.8	0.5	n/a	103
7	2.5	0.8	3.3	0.5	1.4	134
8	3.0	0.8	3.8	0.5	2.3	144
9	3.5	0.8	4.3	0.5	2.8	163
10	4.0	0.8	4.8	0.5	5.9	190
11	4.0	0.5	4.5	1.5	14.4	253
12	3.0	0.5	3.5	1.5	3.0	158
13	2.0	0.5	2.5	1.5	0.7	120
14	2.5	0.5	3.0	1.5	2.6	134
15	3.5	0.5	4.0	1.5	6.5	286
16	2.0	0.8	2.8	1.5	2.3	123
17	2.5	0.8	3.3	1.5	2.9	149
18	3.0	0.8	3.8	1.5	6.2	176
19	3.5	0.8	4.3	1.5	7.5	204
20	4.0	0.8	4.8	1.5	16.1	258

storm surge height (0.5–0.8 m) (Fig. 5), we developed 20 scenarios (Scn) which we used in numerical simulations (Table 2). Data during the incident indicated that water depth was up to the crest level of the seawall (approximately 4 m water depth); therefore, we varied water depth from 2 to 4 m in our simulation scenarios. Regarding wave amplitudes, we referred to the variations at a nearby tide gauge station (West Bay) which showed wave amplitude up to 1.2 m (Fig. 7). Therefore, wave amplitude was varied from 0.5 m to 1.5 m

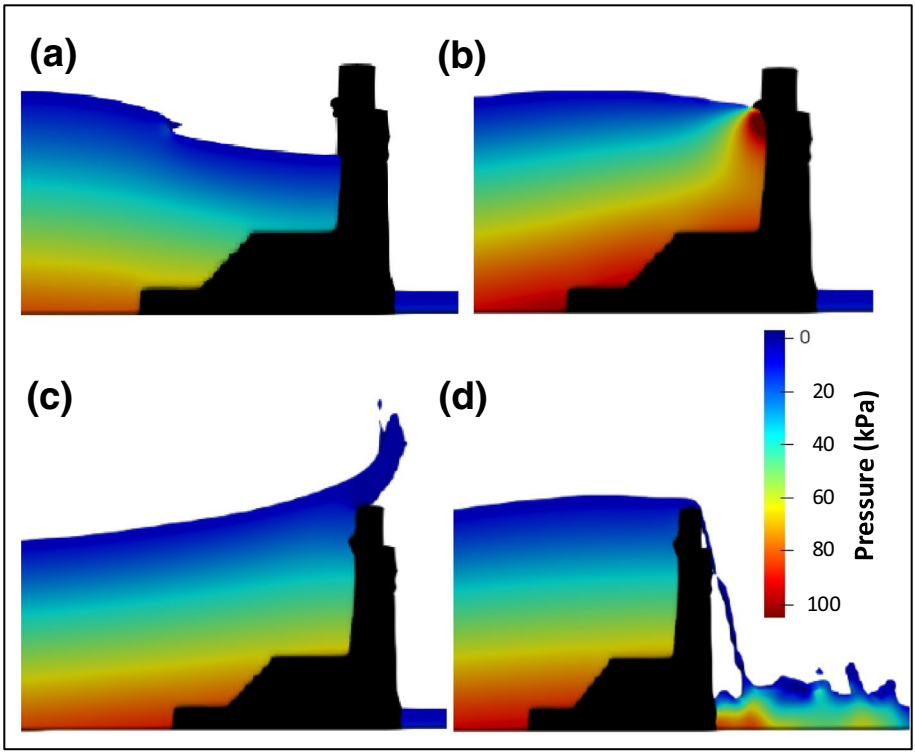

Fig. 8 Wave pressure iso-surface due to Scn-15 (see Table 2 for details of this scenario). **a** Breaking wave at t = 61 s. **b** Maximum breaking pressure at parapet wall t = 61½ s. **c** Wave overtopping wall crown at t = 62 s. **d** Downward overtopping pressure on rail bed t = 63½ s

by considering a factor a safety of 25% for the maximum wave amplitude. As for the storm surge component, time series of storm surges calculated at three coastal stations adjacent to Dawlish showed that it was in the range of 0.5 m to 0.8 m (Fig. 5). These 20 scenarios would help to study uncertainties associated with wave amplitudes and pressures. Figure 8 shows snapshots of wave propagation and impacts on the seawall at different times.

5.1 Results of wave amplitude simulations

Large wave amplitudes can induce significant wave forcing on the structure and cause overtopping of the seawall, which could eventually cascade to other hazards such as erosion of the backfill and scour (Adams and Heidarzadeh, 2021). The first 10 scenarios of our modelling efforts are for the same incident wave amplitudes of 0.5 m, which occur at different water depths (2.0–4.0 m) and storm surge heights (0.5–0.8 m) (Table 2 and Fig. 9). This is because we aim at studying the impacts of effective water depth (d_{eff}—the sum of mean sea level and surge height) on the time histories of wave amplitudes as the storm evolves. As seen in Fig. 9a, by decreasing effective water depth, wave amplitude increases. For example, for Scn-1 with effective depth of 4.5 m, the maximum amplitude of the first wave is 1.6 m, whereas it is 2.9 m for Scn-2 with effective depth of 3.5 m. However, due to intensive reflections and interferences of the waves in front of

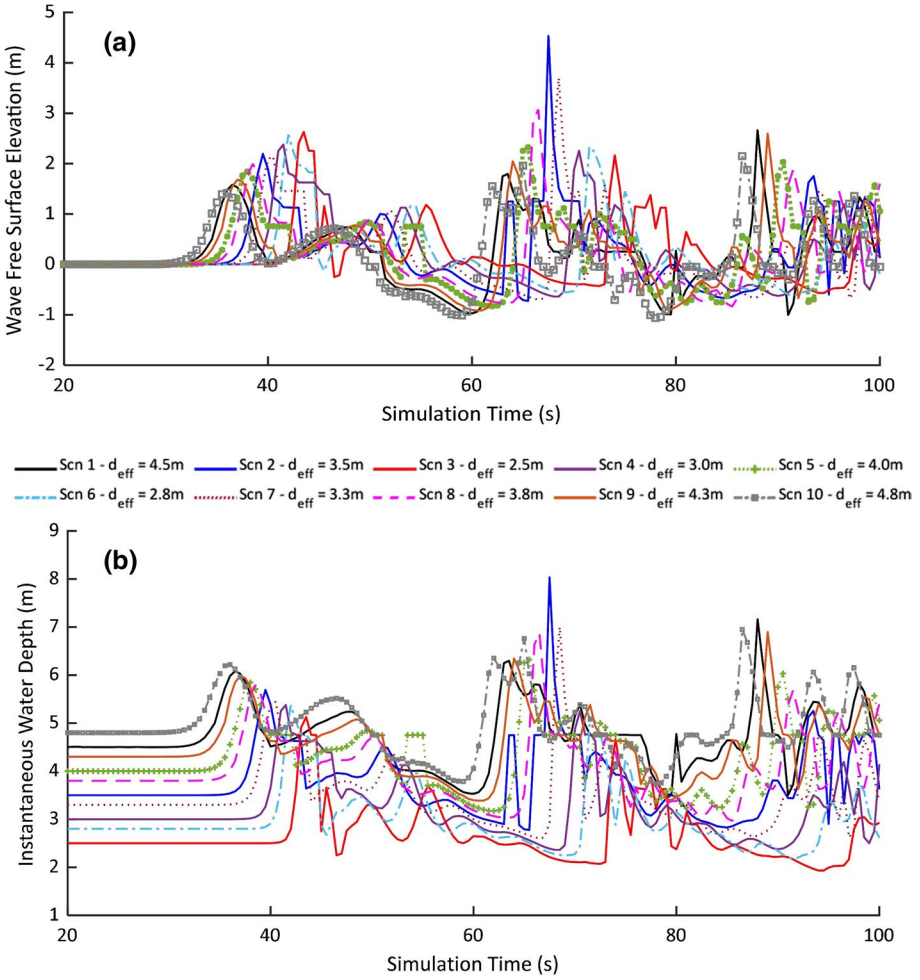

Fig. 9 **a** Time series of wave oscillations at the foot of the seawall (point "A" in Fig. 4) for scenarios 1–10 with incident wave amplitude of 0.5 m. **b** As in "a", but for instantaneous water depth (water depth plus wave amplitude)

the vertical seawall, such a relationship is barely seen for the second and the third wave peaks. It is important to note that the later peaks (second or third) produce the largest waves rather than the first wave. Extraordinary wave amplifications are seen for the Scn-2 ($d_{eff}=3.5$ m) and Scn-7 ($d_{eff}=3.3$ m), where the corresponding wave amplitudes are 4.5 m and 3.7 m, respectively. This may indicate that the effective water depth of $d_{eff}=3.3$–3.5 m is possibly a critical water depth for this structure resulting in maximum wave amplitudes under similar storms. In the second wave impact, the combined wave height (i.e. the wave amplitude plus the effective water depth), which is ultimately an indicator of wave overtopping, shows that the largest wave heights are generated by Scn-2, 7 and 8 (Fig. 9a) with effective water depths of 3.5 m, 3.3 m and 3.8 m and combined heights of 8.0 m, 7.0 m and 6.9 m (Fig. 9b). Since the height of seawall is 5.4 m,

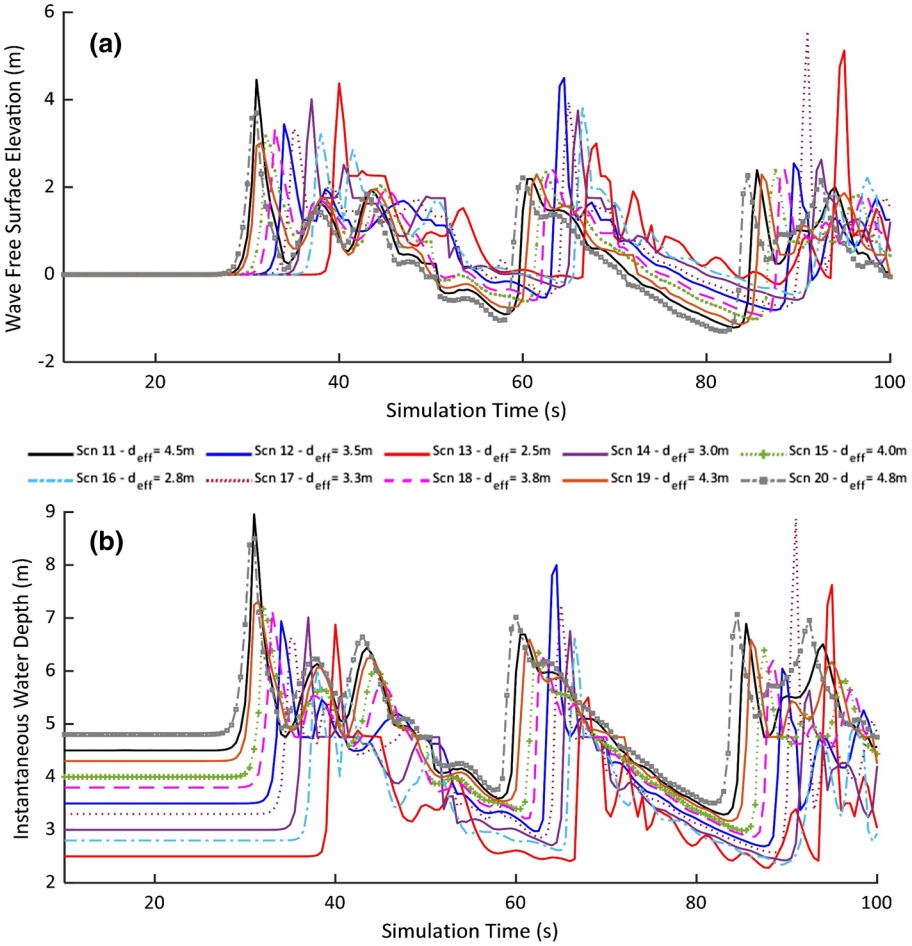

Fig. 10 **a** Time series of wave oscillations at the foot of the seawall (point "A" in Fig. 4) for scenarios 11–20 with incident wave amplitude of 1.5 m. **b** As in "a", but for instantaneous water depth (water depth plus wave amplitude)

the combined wave heights for Scn-2, 7 and 8 are greater than the crest height of the seawall by 2.6 m, 1.6 m and 1.5 m, respectively, which indicates wave overtopping.

For scenarios 11–20 (Fig. 10), with incident wave amplitudes of 1.5 m (Table 2), the largest wave amplitudes are produced by Scn-17 ($d_{eff}=3.3$ m), Scn-13 ($d_{eff}=2.5$ m) and Scn-12 ($d_{eff}=3.5$ m), which are 5.6 m, 5.1 m and 4.5 m. The maximum combined wave heights belong to Scn-11 ($d_{eff}=4.5$ m) and Scn-17 ($d_{eff}=3.3$ m), with combined wave heights of 9.0 m and 8.9 m (Fig. 10b), which are greater than the crest height of the seawall by 4.6 m and 3.5 m, respectively.

Our simulations for all 20 scenarios reveal that the first wave is not always the largest and wave interactions, reflections and interferences play major roles in amplifying the waves in front of the seawall. This is primarily because the wall is fully vertical and therefore has a reflection coefficient of close to one (i.e. full reflection). Simulations

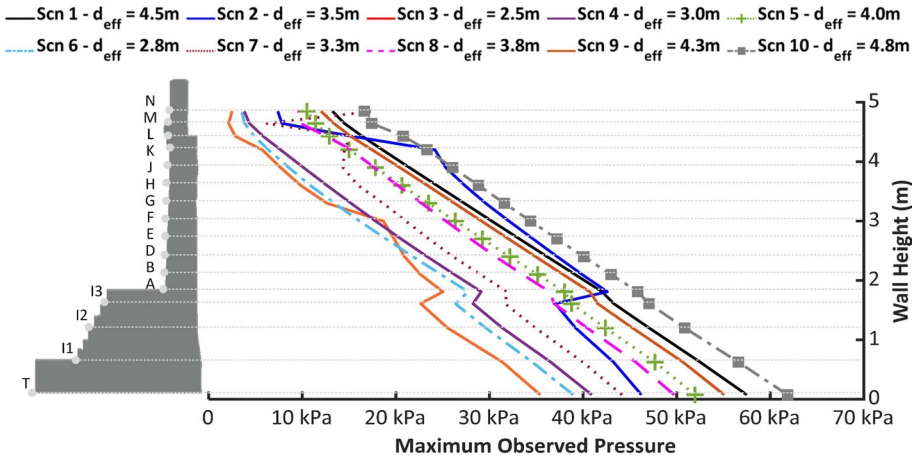

Fig. 11 Distribution of maximum wave pressure along the height of the seawall from scenarios 1–10 with wave amplitude of 0.5 m

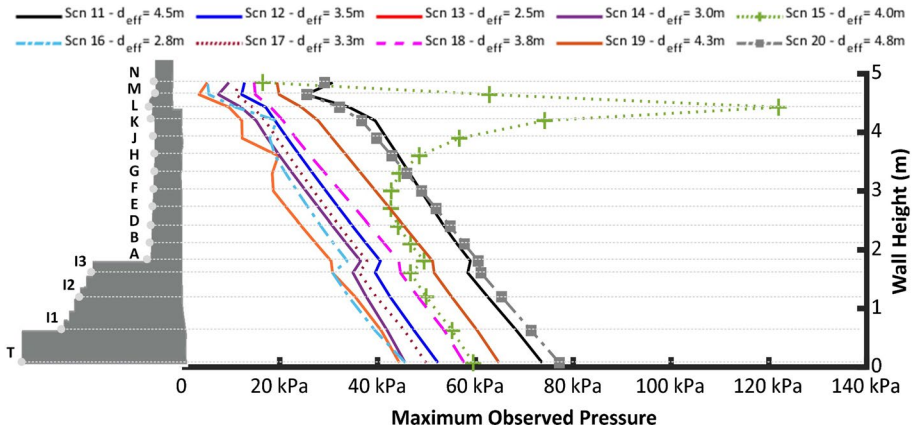

Fig. 12 Distribution of maximum wave pressure along the height of the seawall from scenarios 11–20 with wave amplitude of 1.5 m

show that the combined wave height is up to 4.6 m higher than the crest height of the wall, implying that severe overtopping would be expected.

5.2 Results of wave loading calculations

The pressure calculations for scenarios 1–10 are given in Fig. 11 and those of scenarios 11–20 in Fig. 12. The total pressure distribution in Figs. 11, 12 mostly follows a triangular shape with maximum pressure at the seafloor as expected from the Sainflou (1928) design equations. These pressure plots comprise both static (due to mean sea level in front of the wall) and dynamic (combined effects of surge and wave) pressures. For incident wave amplitudes of 0.5 m (Fig. 11), the maximum wave pressure varies in the range of

35–63 kPa. At the sea surface, it is in the range of 4–20 kPa (Fig. 11). For some scenarios (Scn-2 and 7), the pressure distribution deviates from a triangular shape and shows larger pressures at the top, which is attributed to the wave impacts and partial breaking at the sea surface. This adds an additional triangle-shaped pressure distribution at the sea surface elevation consistent with the design procedure developed by Goda (2000) for braking waves. The maximum force on the seawall due to scenarios 1–10, which is calculated by integrating the maximum pressure distribution over the wave-facing surface of the seawall, is in the range of 92–190 KN (Table 2).

For scenarios 11–20, with incident wave amplitude of 1.5 m, wave pressures of 45–78 kPa and 7–120 kPa, for the bottom and top of the wall, respectively, were observed (Fig. 12). Most of the plots show a triangular pressure distribution, except for Scn-11 and 15. A significant increase in wave impact pressure is seen for Scn-15 at the top of the structure, where a maximum pressure of approximately 120 kPa is produced while other scenarios give a pressure of 7–32 kPa for the sea surface. In other words, the pressure from Scn-15 is approximately four times larger than the other scenarios. Such a significant increase of the pressure at the top is most likely attributed to the breaking wave impact loads as detailed by Goda (2000) and Cuomo et al. (2010). The wave simulation snapshots in Fig. 8 show that the wave breaks before reaching the wall. The maximum force due to scenarios 11–20 is 120–286 KN.

The breaking wave impacts peaking at 286 KN in our simulations suggest destabilisation of the upper masonry blocks, probably by grout malfunction. This significant impact force initiated the failure of the seawall which in turn caused extensive ballast erosion. Wave impact damage was proposed by Adams and Heidarzadeh (2021) as one of the primary mechanisms in the 2014 Dawlish disaster. In the multi-hazard risk model proposed by these authors, damage mechanism III (failure pathway 5 in Adams and Heidarzadeh, 2021) was characterised by wave impact force causing damage to the masonry elements, leading to failure of the upper sections of the seawall and loss of infill material. As blocks were removed, access to the track bed was increased for inbound waves allowing infill material from behind the seawall to be fluidised and subsequently removed by backwash. The loss of infill material critically compromised the stability of the seawall and directly led to structural failure. In parallel, significant wave overtopping (discussed in the next section) led to ballast washout and cascaded, in combination with masonry damage, to catastrophic failure of the wall and suspension of the rails in mid-air (Fig. 1b), leaving the railway inoperable for two months.

5.3 Wave Overtopping

The two most important factors contributing to the 2014 Dawlish railway catastrophe were wave impact forces and overtopping. Figure 13 gives the instantaneous overtopping rates for different scenarios, which experienced overtopping. It can be seen that the overtopping rates range from 0.5 m^3/s/m to 16.1 m^3/s/m (Fig. 13). Time histories of the wave overtopping rates show that the phenomenon occurs intermittently, and each time lasts 1.0–7.0 s. It is clear that the longer the overtopping time, the larger the volume of the water poured on the structure. The largest wave overtopping rates of 16.1 m^3/s/m and 14.4 m^3/s/m belong to Scn-20 and 11, respectively. These are the two scenarios that also give the largest combined wave heights (Fig. 10b).

The cumulative overtopping curves (Figs. 14, 15) show the total water volume overtopped the structure during the entire simulation time. This is an important hazard factor

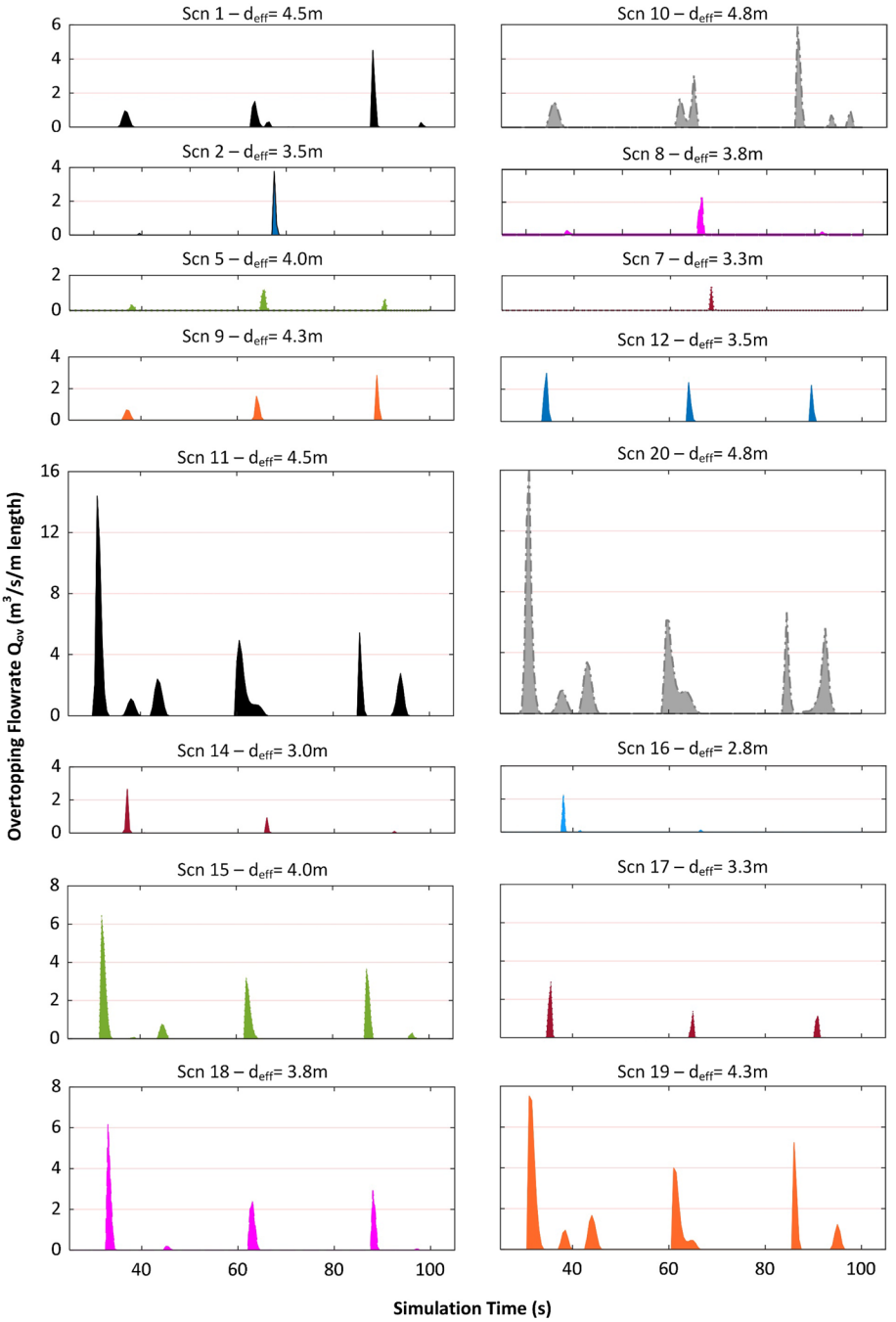

Fig. 13 Wave overtopping rates for all scenarios with overtopping events

as it determines the level of soil saturation, water pore pressure in the soil and soil erosion (Van der Meer et al. 2018). The maximum volume belongs to Scn-20, which is 65.0 m^3/m

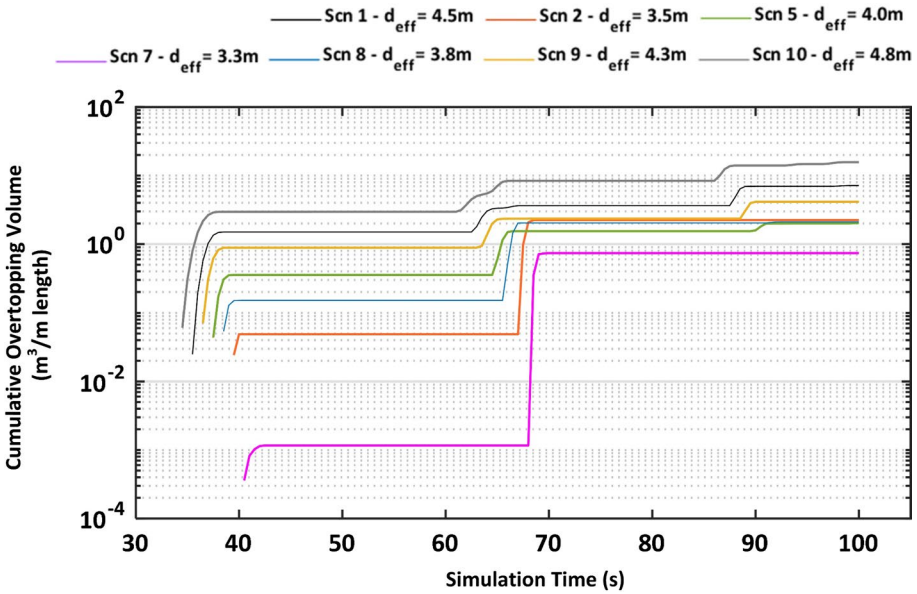

Fig. 14 Cumulative wave overtopping volumes per metre length of wall from scenarios 1–10 with wave amplitude of 0.5 m. No overtopping was experienced in scenarios 3, 4 and 6

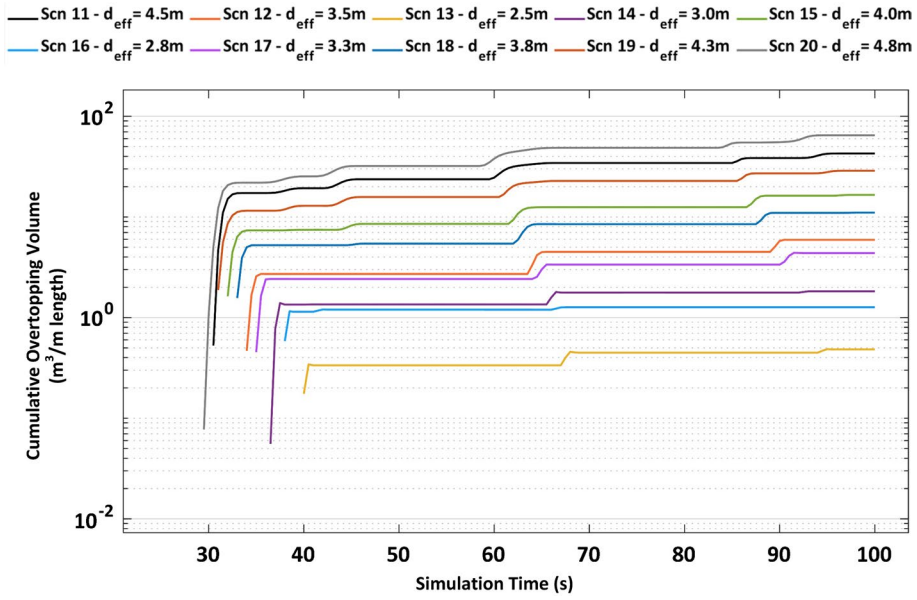

Fig. 15 Cumulative wave overtopping volumes per metre length of wall from scenarios 11–20 with wave amplitude of 1.5 m

(m-cubed of water per metre length of the wall). The overtopping volumes are 42.7 m^3/m for Scn-11 and 28.8 m^3/m for Scn-19. The overtopping volume is in the range of 0.7–65.0 m^3/m for all scenarios.

For comparison, we compare our modelling results with those estimated using empirical equations. For the case of the Dawlish seawall, we apply the equation proposed by Van Der Meer et al. (2018) to estimate wave overtopping rates, based on a set of decision criteria which are the influence of foreshore, vertical wall, possible breaking waves and low freeboard:

$$\frac{q}{\sqrt{gH_m^3}} = 0.0155\left(\frac{H_m}{h_s}\right)^{\frac{1}{2}} e^{\left(-2.2\frac{R_c}{H_m}\right)} \tag{6}$$

where q is the mean overtopping rate per metre length of the seawall (m^3/s/m), g is the acceleration due to gravity, H_m is the incident wave height at the toe of the structure, R_c is the wall crest height above mean sea level, h_s is the deep-water significant wave height and $e^{(x)}$ is the exponential function. It is noted that Eq. (6) is valid for $0.1 < \frac{R_c}{H_m} < 1.35$. For the case of the Dawlish seawall and considering the scenarios with larger incident wave amplitude of 1.5 m (h_s= 1.5 m), the incident wave height at the toe of the structure is H_m = 2.2—5.6 m, and the wall crest height above mean sea level is R_c = 0.6–2.9 m. As a result, Eq. (6) gives mean overtopping rates up to approximately 2.9 m^3/s/m. A visual inspection of simulated overtopping rates in Fig. 13 for Scn 11–20 shows that the mean value of the simulated overtopping rates (Fig. 13) is close to estimates using Eq. (6).

6 Discussion and conclusions

We applied a combination of eyewitness account analysis, sea level data analysis and numerical modelling in combination with our engineering judgement to explain the damage to the Dawlish railway seawall in February 2014. Main findings are:

- Eyewitness data analysis showed that the extreme nature of the event was well forecasted in the hours prior to the storm impact; however, the magnitude of the risks to the structures was not well understood. Multiple hazards were activated simultaneously, and the effects cascaded to amplify the damage. Disaster management was effective, exemplified by the establishment of an emergency rendezvous point and temporary evacuation centre during the storm, indicating a high level of hazard awareness and preparedness.
- Based on sea level data analysis, we identified triple peak period bands at 4–8, 8–12 and 20–25 s in the sea level data. Storm surge heights and wave oscillations were up to 0.8 m and 1.5 m, respectively.
- Based on the numerical simulations of 20 scenarios with different water depths, incident wave amplitudes, surge heights and peak periods, we found that the wave oscillations at the foot of the seawall result in multiple wave interactions and interferences. Consequently, large wave amplitudes, up to 4.6 m higher than the height of the seawall, were generated and overtopped the wall. Extreme impulsive wave impact forces of up to 286 KN were generated by the waves interacting with the seawall.

- We measured maximum wave overtopping rates of 0.5–16.1 m^3/s/m for our scenarios. The cumulative overtopping water volumes per metre length of the wall were 0.7–65.0 m^3/m.
- Analysis of all the evidence combined with our engineering judgement suggests that the most likely initiating cause of the failure was impulsive wave impact forces destabilising one or more grouted joints between adjacent masonry blocks in the wall. Maximum observed pressures of 286 KN in our simulations are four times greater in magnitude than background pressures leading to block removal and initiating failure. Therefore, the sequence of cascading events was :1) impulsive wave impact force causing damage to masonry, 2) failure of the upper sections of the seawall, 3) loss of infill resulting in a reduction of structural strength in the landward direction, 4) ballast washout as wave overtopping and inbound wave activity increased and 5) progressive structural failure following successive tides.

From a risk mitigation point of view, the stability of the seawall in the face of future energetic cyclonic storm events and sea level rise will become a critical factor in protecting the rail network. Mitigation efforts will involve significant infrastructure investment to strengthen the civil engineering assets combined with improved hazard warning systems consisting of meteorological forecasting and real-time wave observations and instrumentation. These efforts must take into account the amenity value of coastal railway infrastructure to local communities and the significant number of tourists who visit every year. In this regard, public awareness and active engagement in the planning and execution of the project will be crucial in order to secure local stakeholder support for the significant infrastructure project that will be required for future resilience.

Acknowledgements We are grateful to Brunel University London for administering the scholarship awarded to KA. The Flow3D-Hydro used in this research for numerical modelling is licenced to Brunel University London through an academic programme contract. We sincerely thank Prof Harsh Gupta (Editor-in-Chief) and two anonymous reviewers for their constructive review comments.

Funding This project was funded by the UK Engineering and Physical Sciences Research Council (EPSRC) through a PhD scholarship to Keith Adams.

Declarations

Conflict of interest The authors have no relevant financial or non-financial interests to disclose.

Availability of data All data used in this study are provided in the body of the article.

References

Ackhurst M (2020) Design of Vertical Gravity Sea and Quay Walls. ICE Publishing, Westminster, London

Adams K, Heidarzadeh M (2021) A multi-hazard risk model with cascading failure pathways for the Dawlish (UK) railway using historical and contemporary data. Int J Disaster Risk Reduc 56:102082. https://doi.org/10.1016/j.ijdrr.2021.102082
BBC (2014a) Dawlish train battered by waves. Accessed 12 May 2022. https://www.bbc.co.uk/news/av/uk-26076630
BBC (2014b) Dawlish storm victim: 'Water coming through our windows'. Accessed 12 May 2022. https://www.bbc.co.uk/news/av/uk-26056696
BBC (2014c) Devon and Cornwall storm: 'Like living in a washing machine'. Accessed 12 May 2022. https://www.bbc.co.uk/news/uk-england-devon-26051900
Brunel Institute (2022) A collaboration between the University of Bristol and the SS Great Britain. DM162/8/1/3/GWR Sketchbook21/folio 10. Accessed on 22 Feb 2022. https://archives.bristol.ac.uk/Record.aspx?src=CalmView.Catalog&id=DM162%2f8%2f1%2f3%2fGWR+Sketchbook+21%2ffolio+10
Courant R, Friedrichs K, Lewy H (1928) Über die partiellen Differenzengleichungen der mathematischen Physik. Math Ann 100(1):32–74
Cuomo G, Allsop W, Bruce T, Pearson J (2010) Breaking wave loads at vertical seawalls and breakwaters. Coastal Eng 57(4):424–439
Dacre HF, Pinto JG (2020) Serial clustering of extratropical cyclones: a review of where, when and why it occurs. Clim Atmos Sci 3:48. https://doi.org/10.1038/s41612-020-00152-9
Dawlish Museum (2015) Dawlish The Great Storm. Video collection, available on DVD at: https://www.devonmuseums.net/The-Great-Storm-DVD/Dawlish-Museum/View-Product/
Dawson D, Shaw J, Gehrels WR (2016) Sea-level rise impacts on transport infrastructure: the notorious case of the coastal railway line at Dawlish, England. J Transport Geog 51:97–109
Feser F, Barcikowska M, Krueger O, Schenk F, Weisse R, Xia L (2015) Storminess over the North Atlantic and northwestern Europe—A review. Quarter J R Meteorol Soc 141:350–382. https://doi.org/10.1002/qj.2364
Flow Science (2022) FLOW3D-Hydro version 1.0.1.3. Accessed 12 Feb 2022. https://www.flow3d.com/products/flow-3d-hydro/
Goda Y (2000) Random seas and design of maritime structures, vol 33. World Scientific Publishing Company
Grinsted A (2008) Tidal fitting toolbox. Accessed 6 Feb 2022. https://uk.mathworks.com/matlabcentral/fileexchange/19099-tidal-fitting-toolbox?focused=3854016&tab=function&s_ tid=gn_loc_drop
Heidarzadeh M, Satake K (2014) Excitation of basin-wide modes of the Pacific Ocean following the march 2011 Tohoku Tsunami. Pure Appl Geophys 171(12):3405–3419. https://doi.org/10.1007/s00024-013-0731-5
Heidarzadeh M, Satake K (2015) Source properties of the 1998 July 17 Papua New Guinea tsunami based on tide gauge records. Geophys J Int 202(1):361–369
Heidarzadeh M, Gusman A, Ishibe T, Sabeti R, Šepić J (2022) Estimating the eruption-induced water displacement source of the 15 January 2022 Tonga volcanic tsunami from tsunami spectra and numerical modelling. Ocean Eng 261:112165. https://doi.org/10.1016/j.oceaneng.2022.112165
Hirt CW, Nichols BD (1981) Volume of fluid (VOF) method for the dynamics of free boundaries. J Comput Phys 39(1):201–225. https://doi.org/10.1016/0021-9991(81)90145-5
Masselink G, Castelle B, Scott T, Dodet G, Suanez S, Jackson D, Floc'h F (2016) Extreme wave activity during 2013/2014 winter and morphological impacts along the Atlantic coast of Europe. Geophys Res Lett 43(5):2135–2143. https://doi.org/10.1002/2015GL067492
Mathworks (2018) MATLAB, 2018. 9.7.0.1190202 (R2019b), Natick, Massachusetts: The MathWorks Inc.
Met Office (2016) Strong winds and flooding from storm Angus. November 2016. Accessed 4 Mar 2022. https://www.metoffice.gov.uk/binaries/content/assets/metofficegovuk/pdf/weather/learn-about/uk-past-events/interesting/2016/strong-winds-and-flooding-from-storm-angus-november-2016---met-office.pdf.
Mölter T, Schindler D, Albrecht AT, Kohnle U (2016) Review on the projections of future storminess over the North Atlantic European Region. Atmosphere 7(4):60. https://doi.org/10.3390/atmos7040060
Network Rail (2014) West of Exeter Route Resilience Study. Accessed 4 May 2022. https://cdn.networkrail.co.uk/wp-content/uploads/2019/05/West-of-Exeter-Route-Resilience-Study-1.pdf
Peninsula Rail Taskforce (2016) Closing the gap: The South West Peninsula strategic rail blueprint. Accessed 4 May 2022. https://peninsularailtaskforce.files.wordpress.com/2016/11/prtf-closing-the-gap.pdf
Rabinovich AB (1997) Spectral analysis of tsunami waves: Separation of source and topography effects. J Geophys Res Oceans 102(C6):12663–12676. https://doi.org/10.1029/97JC00479

Rabinovich AB (2010) Seiches and harbor oscillations. In: Handbook of coastal and ocean engineering, pp 193–236

RMS (2014) RMS White Paper 2013–2014 Winter Storms in Europe: An insurance and catastrophe modelling perspective. Accessed 12 May 2022. https://forms2.rms.com/rs/729-DJX-565/images/ws_2013_2014_europe_winter_storms.pdf

Sainflou G (1928) Essai sur les digues maritimes verticales. Annales de ponts et chaussées, vol 98, tome II, 1928(4):5–48. (**in French**)

Shakou LM, Wybo JL, Reniers G, Boustras G (2019) Developing an innovative framework for enhancing the resilience of critical infrastructure to climate change. Safety Sci 118:364–378. https://doi.org/10.1016/j.ssci.2019.05.019

Van der Meer JW, Allsop NWH, Bruce T, De Rouck J, Kortenhaus A, Pullen T, Schüttrumpf H, Troch P and Zanuttigh B (2018) EurOtop, Manual on wave overtopping of sea defences and related structures. An overtopping manual largely based on European research, but for worldwide application. Available online at: www.overtopping-manual.com.

Wang Y, Su HY, Ren Z, Ma Y (2022) Source properties and resonance characteristics of the tsunami generated by the 2021 M 8.2 Alaska earthquake. J Geophys Res Oceans, 127(3):e2021JC018308. https://doi.org/10.1029/2021JC018308